Fabrication of Well-Organized and Densely Packed Si Nanopillars Containing SiGe Nanodots by Using Block Copolymer Templates

Karim Aissou,[†] Thierry Baron,*[,†] Martin Kogelschatz,[†] Martien Den Hertog,[‡] Jean Luc Rouvière,[‡] Jean-Michel Hartmann,[§] and Bernard Pélissier[†]

Laboratoire des Technologies de la Microélectronique, Centre National de la Recherche Scientifique, 17 Rue des Martyrs, 38054 Grenoble, France, Laboratoire d'Etude des Materiaux par Microscopie Avancee, Commissariat à l'Énergie Atomique/Institute for Nanoscience and Cryogenics, Commissariat à l'Énergie Atomique−Grenoble, 17 rue des Martyrs, 38052 Grenoble Cedex 9, France, and Laboratoire d'Electronique et de Technologies de l'Information, Commissariat à l'Énergie Atomique

Received February 4, 2008. Revised Manuscript Received July 24, 2008

We present a method to obtain a dense array of well-organized SiGe quantum dots in Si nanopillars on a large substrate area by using a PS-*b*-PMMA block copolymer template. First, the 2D order of the template is evaluated using a pair correlation function and a bond-orientational correlation function. It is shown that the holes contained in the polystyrene template form a structure presenting a hexatic order. This template is then used to fabricate the nanopillars using the following method: in a first step, the copolymer template serves as a deposition mask to fabricate a hexagonal array of Pt dots. In a second step, the Pt dot pattern is transferred to an alternation of Si and SiGe layers on a silicon substrate with an anisotropically etching using Cl_2/O_2 plasma.

1. Introduction

Optoelectronics is becoming increasingly important for information and communication technologies. Development of optoelectronic devices that can be integrated with standard microelectronics[1] are of great interest. Actually, light sources and photodetector devices are largely based on direct band gap semiconductor alloys.[2,3] However, it is difficult to incorporate III−V alloys into silicon circuits. By contrast, silicon is a well-known indirect-bandgap semiconductor that is an inefficient light-emitting material. One approach to obtain a light-emitting material is to combine Si with Ge, to form superlattices with quantum wells to adjust the bandgap and reduce nonradiative recombination.[4] However, these heterostructures present a low-intensity photoluminescence at room temperature. This could be enhanced by electron−hole pair localization or confinement in quantum dots.[5,6] Most of the time, SiGe quantum dots are grown randomly on a surface by heteroepitaxy using the Stranski−Krastanov growth mode which does not allow a precise control of the size and the position of the nanostructure.[7]

For device applications, an important challenge that needs to be overcome is to obtain a precise control of the size and the localization of the quantum dots. To do that, we propose to combine epitaxial growth of Si/SiGe 2D heterostructures[8] with the properties of self-assembling diblock copolymer films.[9] The first technique allows to elaborate quantum wells with accurate composition and position in the *z* axis while the second one enables to define SiGe quantum dots by fabricating well-organized (*x* and *y* axes) nanopillars. Vertical nanopillars have already been obtained thanks to cylinder-forming block polymer templates.[10−14] We show here that this technique can also be used to elaborate 3D (*x*, *y*, z axes) organized SiGe quantum dots in Si nanopillars. This method is a generic one and could also be easily extended to many semiconductor heterostructures.

In this work, we use an asymmetric polystyrene-*block*-methyl methacrylate (PS-*b*-PMMA) diblock copolymer to form an organized array of nanostructures with a diameter

* Corresponding author. E-mail: thierry.baron@cea.fr.
[†] LTM-CNRS.
[‡] CEA/INAC.
[§] CEA-LETI.

(1) Hirschmann, K. D.; Tsybeskov, L.; Duttagupta, S. P.; Fauchet, P. M. *Nature* **1996**, *384*, 338.
(2) Ball, P. *Nature* **2001**, *409*, 974.
(3) Baron, T.; Saminadayar, K.; Magnea, N. *Appl. Phys. Lett.* **1995**, *67*, 2972.
(4) Abstreiter, G.; Brugger, H.; Wolf, T.; Jorke, H.; Herzog, H. J. *Phys. Rev. Lett.* **1985**, *54*, 2441.
(5) Apetz, R.; Vescan, L.; Hartmann, A.; Dieker, C.; Lüth, H. *Appl. Phys. Lett.* **1995**, *66*, 445.
(6) Huang, Z.; Wu, Y.; Fang, H.; Deng, N.; Ren, T.; Zhu, J. *Nanotechnology* **2006**, *17*, 1476.
(7) Pchelyakov, O. P.; Bolkhovityanov, Y. B.; Dvurechenski, A. V.; Sokolov, L. V.; Nikiforov, A. I.; Yakimov, A. I.; Voigtländer, B. *Semiconductors* **2000**, *34)*, 1229.
(8) Bozzo, S.; Lazzari, J.-L.; Coudreau, C.; Ronda, A.; Arnaud d'Avitaya, F.; Derrien, J.; Mesters, S.; Hollaender, B.; Gergaud, P.; Thomas, O. *J. Cryst. Growth* **2000**, *216*, 171.
(9) Black, C. T.; Ruiz, R.; Breyta, G.; Cheng, J. Y.; Colburn, M. E.; Guarini, K. W.; Kim, H.-C.; Zhang, Y. *IBM J. Res. Dev.* **2007**, *51*, 605.
(10) Guarini, K. W.; Black, C. T.; Zhang, Y.; Kim, H.; Sikorski, E. M.; Babich, I. M. *J. Vac. Sci. Technol., B* **2002**, *20*, 2788.
(11) Mansky, P.; Huang, Y. L.; Russell, T. P.; Hawker, C. *Science* **1997**, *275*, 1458.
(12) Darling, S. B.; Yufa, N. A.; Cisse, A. L.; Bader, S. D.; Sibener, S. J. *Adv. Mater.* **2005**, *17*, 2446.
(13) Thurn-Albrecht, T.; Schotter, J.; Kastle, G. A.; Emley, N.; Shibauchi, T.; Krusin-Elbaum, L.; Guarini, K.; Black, C. T.; Tuominen, M. T.; Russell, T. P. *Science* **2000**, *290*, 2126.
(14) Aissou, K.; Pascale, A.; Kogelschat, M.; Baron, T. Private communication, to be published.

10.1021/cm800364t CCC: $40.75
Published on Web 09/23/2008

of 20 nm and a periodicity of 40 nm. First, the translational and the orientational order of the pattern are evaluated quantitatively by applying a pair correlation and a bond-orientational correlation function. This pattern is then used to generate a hexagonal array of metallic nanodots thanks to a lift-off process. Finally, the metallic dot array is used as an etching mask to obtain ordered SiGe quantum dots in Si nanopillars.

2. Experimental Section

For the present demonstration, a Si(10 nm)/$Si_{0.8}Ge_{0.2}$(10 nm) superlattice is first of all epitaxially grown on a Si(100) substrate by reduced pressure chemical vapor deposition and capped by a thin silicon dioxide (2 nm) layer. To fabricate ordered nanopillars containing the quantum dots, the self-assembling properties of an asymmetric polystyrene-*block*-methyl methacrylate (PS-*b*-PMMA) diblock copolymer from Polymer Source Inc., having a PMMA weight fraction of 0.3 with a molecular weight (M_w) of 67100 g mol^{-1} and a polydispersity of 1.09 is used as received. To prepare films with vertical PMMA cylinders in a PS matrix, the substrate is modified such that there are no preferential interactions with any of the polymer blocks. So, a 1% (w/w) toluene diluted hydroxy-terminated random copolymer of styrene and methyl methacrylate (from Polymer Source Inc.), denoted PS-*ran*-PMMA, having a PS weight fraction of 0.59, a M_w of 13100 g mol^{-1}, and a polydispersity of 1.47 is deposited by spin coating on the thin silicon dioxide layer (2 nm).[11] Thermal annealing under vacuum ($\sim 1 \times 10^{-2}$ mbar) at 170 °C for 3 days are used to anchor the film, followed by a toluene washing to eliminate the excess of polymer. Then, a thin ($\sim$39 nm) film of PS-*b*-PMMA diblock copolymer is deposited on the substrate by spin-coating a toluene diluted solution (1% w/w) followed by annealing at 170 °C for 3 days. The samples are then exposed to ultraviolet (UV) light (HgXe, $\sim$1,2 J/cm^2) during 15 min and rinsed in acetic acid to remove the PMMA phase, leaving an hexagonal array of holes in the PS matrix. Indeed, the PMMA is degraded via a chain scission under UV irradiation whereas the PS is cross-linked and becomes insoluble.[12,13] To remove the PS-*ran*-PMMA brush layer contained at the bottom of the holes, the sample is then exposed to a reactive ion etching (RIE) plasma. The etching process is performed under O_2 (20 sccm) at a pressure of 93 mTorr with 10 W RF power and 150 V bias during 20 s in a Nextral etch tool. Then, a 5 nm thick layer of Pt is deposited onto the PS mask by dc magnetron sputtering under an Ar pressure of 2.0 mTorr at ambient temperature. The typical deposition rate, obtained under a current of 100 mA and a voltage of 340 V applied to each target,is 1.0 Å s^{-1}. In order to realize the lift-off process, we expose the sample to a inductive coupled plasma (ICP) plasma (LAM 9400). An Ar (50 sccm) plasma at 4.2 mTorr pressure with 350 W source power and 70 W bias power is then used during 45 s to selectively remove the excess metal layer on the top of the PS matrix. The residual polymer template is removed with an O_2 (80 sccm) plasma at a pressure of 10 mTorr with 200 W RF power and 50 W bias power during 40 s. These Pt dots serve as a hard mask to fabricate an ordered array of Si/$Si_{0.8}Ge_{0.2}$/Si or Si/$Si_{0.8}Ge_{0.2}$/Si/$Si_{0.8}Ge_{0.2}$/Si nanopillars by etching {Si 10 nm/$Si_{0.8}Ge_{0.2}$ 10 nm} superlattices with a Cl_2/O_2 ICP plasma. The process conditions are Cl_2(180 sccm)/O_2(x sccm with $0 \leq x \leq 25$), 5 mTorr, 300 W source power, and 90 W bias power. For more clarity, the lift-off process and the pillar fabrication using the Pt dots as a hard mask are shown in Figure 1 for a Si/$Si_{0.8}Ge_{0.2}$/Si/$Si_{0.8}Ge_{0.2}$/Si stack case. As compared to a process that use PS as the minority phase and hence PS pillars as etching mask, the Pt hard mask presents the advantage to be not consume during the plasma etching procedure.

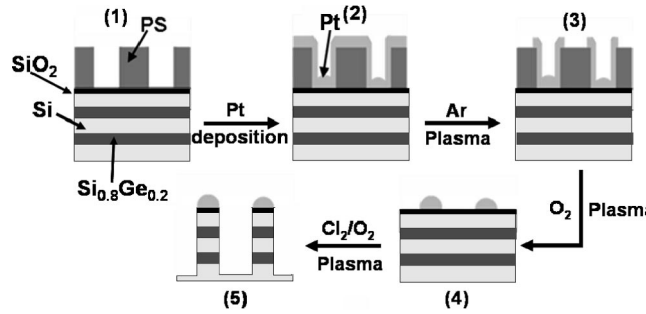

Figure 1. Schematic process flow for Pt dots fabrication by lift-off technique and realization of pillars by using Pt dots as a hard mask: (1) PS porous template on a SiO_2/Si/$Si_{0.8}Ge_{0.2}$/Si/$Si_{0.8}Ge_{0.2}$/Si multilayer, (2) Pt deposition onto the mask, (3) Ar plasma to selectively remove the metal in excess on top of the PS layer, (4) O_2 plasma to remove the residual polymer and side-walls metal-coated PS, and (5) etching the multilayer with a Cl_2/O_2 ICP plasma

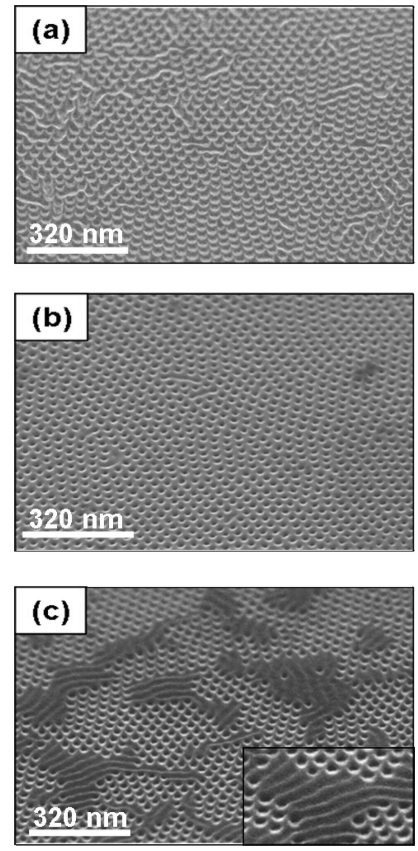

Figure 2. SEM images (40° tilted views) of a 54 nm thick PS-*b*-PMMA film annealed under vacuum during 24 h at different temperatures (after the removal of the PMMA cylinders): (a) 150, (b) 170, and (c) 250 °C. The inset in (c) shows a zoomed view on the horizontal cylinder phase.

3. Results and Discussions

3.1. Evolution and Evaluation of 2D Order. We have studied the effect of the annealing temperature ($T_{annealing}$) (150 °C-250 °C during 24 h) on the self-assembling of PS-*b*-PMMA films having an initial thickness of 54 nm. Typical SEM (scanning electron microscopy) images of these films are shown in Figure 2. For the film annealed at 150 °C

(Figure 2a), the presence of vertical cylinders ordered in a hexagonal array is observed in coexistence with horizontal cylinders. Horizontal cylinders are less present in film annealed at 170 °C (Figure 2b). Indeed, by increasing $T_{annealing}$, horizontal cylinders are consumed to form the vertical cylinder phase ($C_\perp$) which occupies almost all of the film volume. As $T_{annealing}$ reaches 250 °C (Figure 2c), horizontal cylinders appear again to occupy a greater fraction of the image than those observed in Figure 2b. As shown in the insert of the Figure 2c, horizontal cylinders are dug deeper into the film than those shown in Figure 2a. This is the reason why horizontal cylinders appear darker than the vertical ones. In a previous work,[14] we have established that the self-assembling mechanism of the PS-*b*-PMMA proceeds via two consecutive steps. The first mechanism could be resumed to the local segregation of domains which leads to a metastable disordered cylinder phase (C_d) presenting horizontal cylinders. The second mechanism is a transformation of the C_d phase into a vertical cylinder phase via a nucleation-growth mechanism. The results presented here show that there is a range of temperature in which the transformation from the C_d phase into the $C_\perp$ phase is optimal (160−200 °C). This phenomenon is due to a competition between thermodynamic and kinetic requirements.[15]

Figure 3 presents a typical SEM image of organized film and its associated Delaunay triangulation for optimized process conditions (film thickness of 39 nm,[16] annealing temperature of 170 °C). On this triangulation, we observe well-organized areas, here after called "grains" in reference to polycrystalline terminology, corresponding to regions where all cylinders are 6-fold coordinated (blue dots). Cylinders with seven neighbors (green dots) and those with five neighbors (red dots) correspond to defects that separate grains presenting an anisotropic shape and a specific orientation. These defects are called dislocations when they are formed by a pair of 5−7 coordinated cylinders (indicated by a connected yellow bar) or are called disclinations when defects are unpaired (indicated by a circled star).[17]

To evaluate the 2D order of the film shown in Figure 3a, we have plotted the pair correlation function $g(r)$ (Figure 4a) and the bond-orientational correlation function $G_6(r)$ (Figure 4b) obtained thanks to the method proposed by Quinn et al.[18] The pair correlation function $g(r)$ represents the probability of finding two cylinders separated by a distance r. It measures the translational order in the structure and is defined as

$$g(r) = \frac{1}{\rho^2}\left\langle \sum_i \sum_{j\neq i} \delta(r_i)\delta(r_j - r)\right\rangle$$

where ρ and r_i are the mean cylinder density and the positional vector of the cylinder i. The normalized bond-orientational correlation function measures the orientational order in the structure, based on the principle that all bonds in a perfect hexagonal lattice should have the same angle, modulo $\pi/3$, with respect to an arbitrary axis. It is given by

$$G_6(r) \equiv \langle \psi_6^*(r)\psi_6(0)\rangle / G_B(r)$$

where $G_B(r)$ is the autocorrelation function of the bond density and $\psi_6(r)$ is the bond-orientational order parameter given by

$$\psi_6(r) \equiv \sum_{r_{jk}} \delta(r - r_{jk})\exp(6i\varphi_{jk})$$

where r_{jk} is the position vector of the bond center linking j and k cylinders and ϕ_{jk} is the angle between the bond connecting the cylinders j and k and the x arbitrary axis. To use the KTHNY (Kosterlitz−Thouless−Halperin−Nelson−Young) predictions reported in Table 1, we have fitted $g(r)$ and $G_6(r)$ data with exponential and power functions. The envelope of $g(r)$ can be fitted by an exponential decay ($\exp[-r/\xi_p]$) with $\xi_p = (7.6 \pm 0.6)\ p$ (p is the lattice period), which indicates a short-range translational order. We have

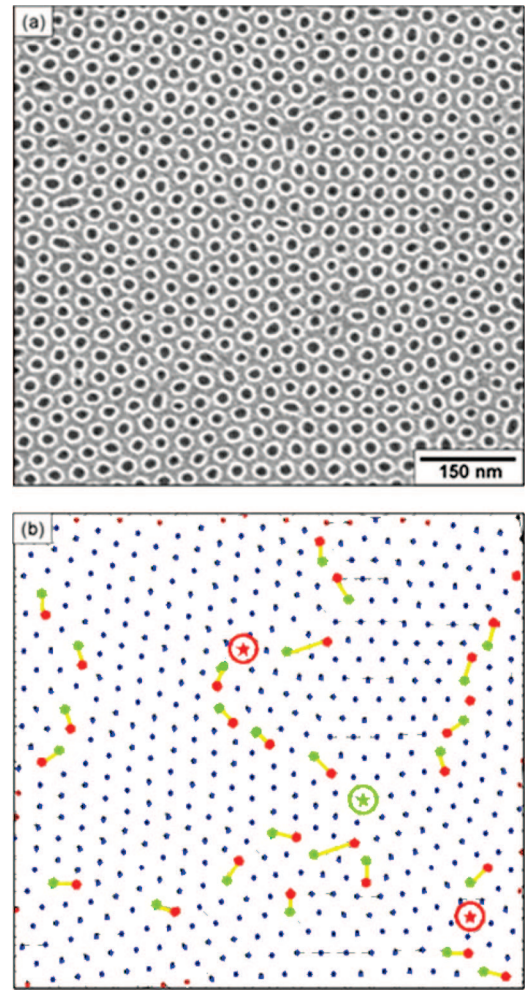

Figure 3. (a) SEM image (plan view) of a 39 nm thick PS-*b*-PMMA film annealed during 24 h at 170 °C under a vacuum and after the removal of PMMA cylinders and (b) its Delaunay triangulation. Well-organized grains correspond to regions where all cylinders are 6-fold coordinated (blue dots). These grains are delimited by 7-fold (green dots and encircled stars) and 5-fold (red dots and encircled stars) coordinated cylinders. Dislocations formed by a pair of 5−7 disclinations are indicated by a connecting yellow bar.

(15) Yokoyama, H.; Mates, T. E.; Kramer, E. J. *Macromolecules* **2000**, *33*, 1888.
(16) In ref 14, we show that the kinetics of vertical cylinder formation is optimal when the film thickness tend to the natural cylinder monolayer thickness.
(17) Aissou, K.; Baron, T.; Kogelschatz, M.; Pascale, A. *Macromolecules* **2007**, *40*, 5054.
(18) Quinn, R. A.; Cui, C.; Goree, J.; Pieper, J. B.; Thomas, H.; Morfill, G. E. *Phys. Rev. E* **1996**, *53*, R2049.

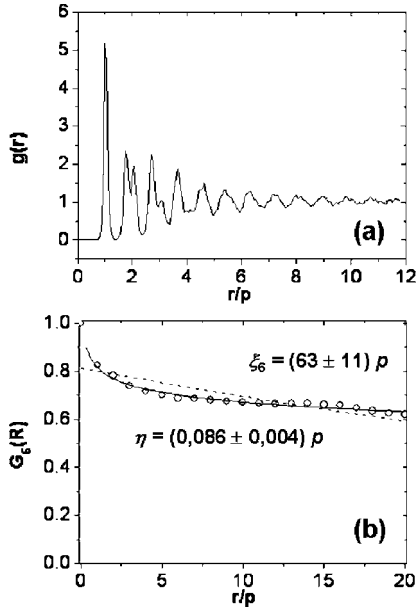

Figure 4. (a) Pair correlation and (b) bond-orientational correlation functions associated to the film shown in Figure 3a versus normalized distance *r*/*p*. In (a), the envelope of the curve can be fitted by an exponential law. In (b), $G_6(r)$ data (open circles) are fitted with an exponential and a power law corresponding to the dashed and the full curves.

Table 1. Criteria of the KTHNY Theory, Applied to $g(r)$ and $G_6(r)$ Functions, Allowing Us To Distinguish the Different Phases[a]

	crystalline phase	hexatic phase	isotropic phase
$g(r)$	$g(r) \approx r^{-\eta}$ with $0 < \eta \leq 1/3$	$g(r) \approx \exp(-r/\xi_p)$	$g(r) \approx \exp(-r/\xi_p)$
$G_6(r)$	$G_6(r) \equiv 1$	$G_6(r) \approx r^{-\eta}$ with $0 < \eta \leq 1/4$	$G_6(r) \approx \exp(-r/\xi_6)$

[a] ξ_p and ξ_6 represent the length of positional and orientational correlation, respectively.

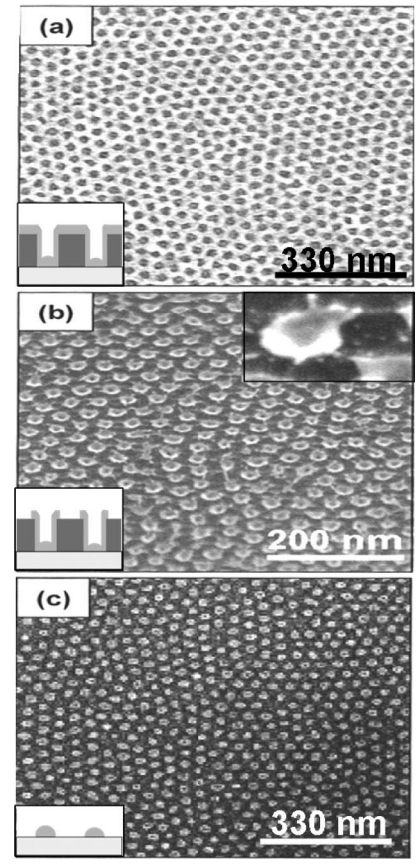

Figure 5. SEM images (a) after the deposition of a 5 nm thick Pt layer on a mask of holes in a PS matrix, (b) after the removal of Pt on top of the PS matrix using an Ar plasma, and (c) after the removal of the residual polymer and Pt-coated PS on the sidewalls by an O_2 plasma. The Pt dots have a mean diameter of around 20 nm and a center-to-center distance of 40 nm.

also fitted the $G_6(r)$ data with an exponential decay (exp $[-r/\xi_6]$) and a power decay ($r^{-\eta}$). We have found an orientational correlation length $\xi_6 = (63 \pm 11)p$ and a power exponent $\eta = (0.086 \pm 0.004)\ p$, which indicates a quasi long-range orientational order. From these results, we find that $\xi_p < \xi_6$ and $\eta < 0.25$, showing that the structure is a hexatic phase.[16]

3.2. Fabrication of Si/SiGe Nanopillar Arrays. Figure 5 presents the different technological steps to fabricate a hexagonal array of Pt dots, with a diameter of 20 nm and a periodicity of 40 nm. It gives a nanostructure density around 1×10^{11} cm^{-2}. A 5 nm thick Pt continuous layer is deposited onto the PS mask (Figure 5a). The metal dot lift-off process is then realized as followed. An Ar ICP plasma is employed to selectively remove the excess metal layer on top of the PS matrix (Figure 5b). The residual PS polymer and Pt on the sidewalls are removed by an oxygen plasma (Figure 5c), leaving the surface with a 2D hexagonal array of Pt dots.

The fabrication of vertical nanowires containing the SiGe quantum dots is obtained through a transfer of the metallic mask into a Si/SiGe multilayer. A process which allows to anisotropically etch both Si and $Si_{0.8}Ge_{0.2}$ layers is used. The etching recipe has been adapted from a $HBr/Cl_2/O_2$ process used to etch polycrystalline silicon gates. Etching of Si/SiGe gates with these kinds of chemistries has been studied by Vallon et al.[19] They found that using a $HBr/Cl_2/O_2$ chemistry led to an important preferential lateral etching of SiGe in comparison to Si. The removal of HBr from the etch chemistry allowed to greatly reduce the preferential etching of SiGe. This phenomenon was attributed to a higher reactivity of the halogen atoms with respect to the SiGe layers than with respect to the Si layers. We have thus used Cl_2/O_2 plasmas to anisotropically etch our Si/SiGe stacks.

Figure 6 shows SEM images of pillars etched to a Si/$Si_{0.8}Ge_{0.2}$/Si/$Si_{0.8}Ge_{0.2}$/Si stack with a Cl_2/O_2 plasma with an O_2 flow of 20 sccm. Figure 6a shows that the Pt dots have been completely removed by this etching step. This is due to a lateral etching of the $Si_{0.8}Ge_{0.2}$ layers which leads to the removal of the top layers. As shown in the next section, this effect could be avoid by adjusting the Cl_2/O_2 ratio to limit the lateral SiGe etching. The hexagonal coordination of the pillars (a hexagon was added on Figure 6a) confirms that the pillars have been formed by a transfer of the Pt dot mask to the substrate. Figure 6b shows pillars having different height. This effect is attributed to a lift-off mechanism occurring either at the first or the second $Si_{0.8}Ge_{0.2}$ layer which changes the height of the pillars. If both $Si_{0.8}Ge_{0.2}$ layers are lifted the pillar is smaller (solid arrows) than in

(19) Vallon, S.; Monget, C.; Joubert, O.; Vallier, L.; Bell, F. H.; Pons, M.; Regolini, J. L.; Morin, C.; Sagnes, I. *J. Vac. Sci. Technol., A* **1997**, *15*, 1874.

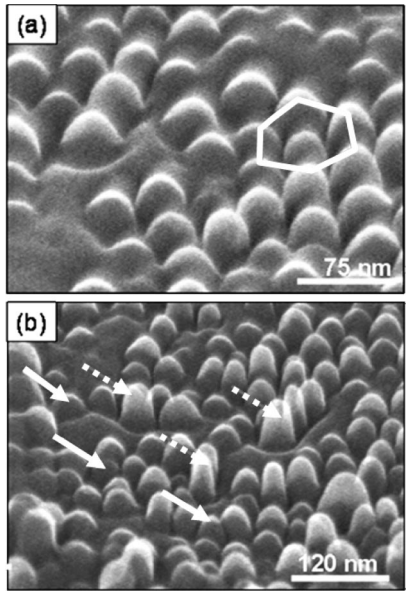

Figure 6. SEM images obtained after transfer of the Pt dot mask to a {10 nm thick Si/10 nm thick $Si_{0.8}Ge_{0.2}$/10 nm thick Si/10 nm thick $Si_{0.8}Ge_{0.2}$/Si substrate} stack thanks to an anisotropic etching with a Cl_2(180 sccm)/O_2(20 sccm) plasma. (a) Hexagonal structure indicated by a light hexagon shows that the pillars result from the Pt dot mask. The absence of Pt dots is due to the lateral etching of the $Si_{0.8}Ge_{0.2}$ layer. (b) High pillars (dashed arrows) are formed when only the upper SiGe layer has been etched. If both SiGe layers have been removed, low pillars are formed (full arrows).

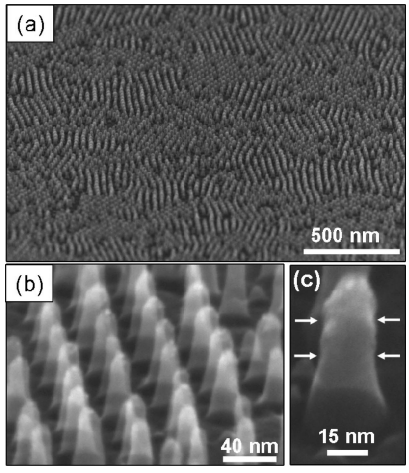

Figure 7. SEM images of pillars obtained by the transfer of the Pt dot mask to a {10 nm thick Si/10 nm thick $Si_{0.8}Ge_{0.2}$/10 nm thick Si/10 nm thick $Si_{0.8}Ge_{0.2}$/Si substrate} stack with a Cl_2(180 sccm)/O_2(25 sccm) chemistry at different magnifications: (a) Grains of pillars having different orientations, (b) pillars contained in the same grain and (c) an isolated ~50 nm tall pillar. The arrows are showing that the diameter of the SiGe layers is lower due to lateral etching.

the case where only one SiGe layer is lifted (dashed arrows). The lifting of the Pt dots was observed for O_2 flow rates $\leq$20 sccm.

Figure 7 shows nanopillars etched to a Si/$Si_{0.8}Ge_{0.2}$/Si/$Si_{0.8}Ge_{0.2}$/Si stack with a Cl_2(180 sccm)/O_2(25 sccm) ICP plasma during 15 s. On the low magnification image of Figure 7a, different areas or grains can be seen. In each grain, nanopillars have an hexagonal array. The orientation of the hexagonal arrays change from one grain to the other one. Figure 7b shows a zoom on a grain. On this figure, it can be seen that all the pillars have a cylindrical shap with the same height (~50 nm) and diameter (~20 nm). The Pt dots are still present after the etching step. This means that the increase of the O_2 flow rate in the etching gas limits the lateral etching of $Si_{0.8}Ge_{0.2}$quantum dots. Nerveless, Figure 7c shows that the diameter of the pillar is lower at the locations of the $Si_{0.8}Ge_{0.2}$ layers. The significant decrease of the lateral etching of $Si_{0.8}Ge_{0.2}$ layers with the increasing O_2 flow is due to a passivation of the pillar-sidewalls by an oxide layer.[20] The thinner diameter of the $Si_{0.8}Ge_{0.2}$ regions of the nanopillars is attributed to a thinner passivation layer on these $Si_{0.8}Ge_{0.2}$ regions than on the Si regions of the nanopillars. This effect was also observed by Monget et al.[24] By analyzing the composition of the passivation layer by X-ray Photoelectron Spectroscopy, they have shown that its composition was Si−O−Cl. As no germanium could be detected, they concluded that germanium etch products desorb into the gas phase without redepositing on the sidewalls. This means that only silicon contributes to formation of the passivation layer, which is consequently thinner on the SiGe layers than on the Si layers.

The evolution of the lateral etching of the $Si_{0.8}Ge_{0.2}$ quantum dots as a function of the O_2 flow can be explained as a competition between lateral etching due to a high reactivity of germanium with oxygen and the formation of a passivation layer. In our case, we can conclude that for O_2 flow rates $\leq$20 sccm the lateral etching of $Si_{0.8}Ge_{0.2}$ quantum dots dominates and that at 25 sccm of O_2 the passivation layer becomes thick enough to reduce it. The lifting of the Pt dots as shown in Figure 6 was even observed in the case of a plasma without oxygen addition. This can be explained by the erosion of the quartz window of the reactor, leading to the formation of oxygen atoms that can react with SiGe[24].

To access to the physicochemical nature of the nanopilars after the etching process, we performed XPS measurements on the samples (spectra not shown here). The Si spectrum shows two contributions at 99.6 and 104 eV, commonly attributed to Si−Si and Si−O bounding environment respectively. The Ge 2p electronic level shows Ge−Ge and Ge−O contributions at 1218 and 1221.5 eV, respectively.[21] An interesting point to note here is that the 1221.5 eV peak corresponds to a completely oxidized Germanium state[22] with no significant suboxide. The presence of the Ge−Ge and Si−Si peaks shows that the Ge structure of the nanopillar is still present after the etching whereas the Ge−O and Si−O contribution is very likely due to the passivation layer on the sidewall. The high reactivity of the oxygen radicals present in the gas phase during plasma process explains the completed oxidized Ge state observed here.

To characterize accurately the composition, the thickness, as well as the crystalline quality of the multilayer after etching process, in Figure 8a we show a typical high resolution transmission electron microscopy (HR-TEM)

(20) Monget, C.; Vallon, S.; Bell, F. H.; Vallier, L.; Joubert, O. *J. Electrochem. Soc.* **1997**, *144*, 2455.
(21) Moulder, J. F.; Stickle; W. F., Sobol, P. E.; Bomben, K. D. *Handbook of X-ray Photoelectron Spectroscopy*; Perkin-Elmer Corp.: Eden Prairie, MN, 1992.
(22) Pelissier, B.; Kambara, H.; Godot, E.; Veran, E.; Loup, V.; Joubert, O. *Microelectron. Eng.* **2008**, *85*, 151.

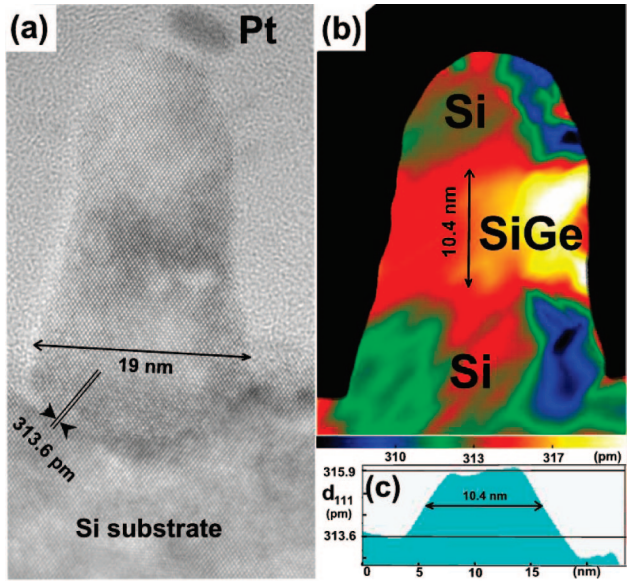

Figure 8. (a) HRTEM image of a nomimal {10 nm thick Si/10 nm thick $Si_{0.8}Ge_{0.2}$/Si subtrate} nanopillar elongated along the vertical ⟨001⟩ direction. Image is taken along a lateral ⟨110⟩ direction. Note the remains of the Pt dot mask (dark particle). This Pt mask is not touching the nanopillar indicating that either it has been displaced or that part of the top of the nanopillar has been slightly edged during the TEM sample preparation. Two (111) planes separated by 313.6 pm are outlined near the Si substrate. A slight etching of the SiGe layer can be noticed. (b) (111) interplanar distance map in pm obtained from Figure 8a by using the Geometrical phase Analysis. The distances have been averaged over large areas (5×5 nm^2) and the measures at the edge of the wires are partly biased (averaged areas include vacuum). The regions where no (111) lattice fringes have been detected have been masked (dark areas) in order to suppress the noise in these regions. (c) (111) interplanar distance profile extracted along the central vertical stripe of (b). The variation of the (111) lattice plane are clearly seen. In this profile, the width of the $Si_{1-x}Ge_x$ layer is measured equal to 10.4 nm and the distance of 315.9 pm corresponds to the (111) interplanar distance of a $Si_{84}Ge_{16}$ compound biaxially stressed by a Si layer.

image of a nanopillar containing the following multilayer: 10 nm thick Si/10 nm thick $Si_{0.8}Ge_{0.2}$/Si substrate. This image was obtained with a JEOL 4000EX microscope. Cross-sections of samples were realized by gluing the surface containing the Si/SiGe nanopillars with a dummy piece of Si. A very liquid glue was used. Cross-sections were classically prepared by mechanical polishing and ion milling (Gatan PIPS ion miller). No defects were observed in the nanopillars and, as shown in Figure 8a, the crystallographic structure of the nanopillars is perfect. A slight reduction in the diameter of the nanopillar can be noticed in the SiGe layer: at the base of the nanopillar, the diameter is 19 nm, whereas it is 15 nm in the SiGe layer. To evaluate the Ge content of the SiGe region, local lattice parameters have been measured by using the geometrical phase analysis (GPA).[23] Figure 8b shows a lattice parameter map of the (111) planes. This d_{111} map clearly shows the SiGe layer. Depending on the analyzed HRTEM images, the thickness of the SiGe layers was measured varying from 10 to 11.1 nm and the Ge chemical composition was found between 15 and 18%, which is quite in agreement with the nominal value of 20%. The Ge composition was measured by assuming that the (111) interplanar distance d_{111} of the Si region is equal to 313.6 pm (bulk value of Si) and that the $Si_{1-x}Ge_x$ layer was biaxially stressed by the Si substrate and the Si layers. For instance in Figure 8c, a distance of 315.9 pm correspond to a Ge chemical composition of 16% is found. The accuracy in the measure of (111) interplanar distances averaged over large areas (5×5 nm^2) is about 0.5 pm, which corresponds to an accuracy of about 2% in the Ge composition, but additional errors due to surface relaxation and specimen preparation can be added. All this analysis indicates that the etching process has not damaged the original layered structure.

4. Conclusions

We have developed a method to obtain an array of well-organized, densely packed Si nanopillars containing SiGe quantum dots by using a PS-*b*-PMMA block copolymer template. The typical final size is a cylinder presenting radius and thickness of 10 nm. The density of the pillar is around 1×10^{11} cm^{-2}. First, the 2D order of the porous PS template was evaluated using a pair correlation function and a bond-orientational correlation function. It was found that the structure of holes is a hexatic phase. Then, in a first step, the copolymer template was used as a deposition mask to obtain a hexagonal array of Pt dots. In a second step, the metal dots were used as a hard mask to develop a Cl_2/O_2 plasma etch process, which allows to etch anisotropically the Si/$Si_{0.8}Ge_{0.2}$ stack without damaging the original structure. It is shown that the Cl_2/O_2 ratio has to be well-adjusted to allow the formation of a passivation layer on the cylinder sidewalls and thus avoid the lateral etching of the $Si_{0.8}Ge_{0.2}$ layers.

Acknowledgment. We are grateful to G. Cunge, O. Joubert, and B. Salem from LTM-CNRS for helpful discussions as well as to the platform of CEA-LETI for technological support.

CM800364T

(23) Rouvière, J. L.; Sarigiannidou, E. *Ultramicroscopy* **2005**, *106*, 1.